

Blind MD-MC component separation for polarized observations of the CMB with the EM algorithm

J. Aumont, J. F. Macías-Pérez

Laboratoire de Physique Subatomique et de Cosmologie, 53 Avenue des Martyrs, 38026 Grenoble Cedex, France

3 November 2018

ABSTRACT

We present in this paper the PoLEMICA (Polarized Expectation-Maximization Independent Component Analysis) algorithm which is an extension to polarization of the SMICA temperature MD-MC component separation method. This algorithm allows us to estimate blindly in harmonic space multiple physical components from multi-detectors polarized sky maps. Assuming a linear noisy mixture of components we are able to reconstruct the electromagnetic spectra of the components for each mode T , E and B , as well as the temperature and polarization spatial power spectra, TT , EE , BB , TE , TB and EB for each of the physical components and for the noise on each of the detectors. PoLEMICA is specially developed to estimate the CMB temperature and polarization power spectra from sky observations including both CMB and foreground emissions. This has been tested using full sky simulations of the Planck satellite polarized channels for a 14-months nominal mission assuming a simple linear sky model including CMB, and optionally Galactic synchrotron and dust emissions. From this analysis we conclude that although the foreground contribution can be removed, it reduces significantly the precision to which the CMB polarization can be measured.

Key words: – Cosmic microwave background – Cosmology: observations – Methods: data analysis

1 INTRODUCTION

Mapping the Cosmic Microwave Background (CMB) polarization is one of the major challenges of future missions of observational cosmology. CMB polarization is linear and therefore can be described by the first three Stokes parameters I , Q and U which are generally combined to produce three fields (modes), T , E and B (Zaldarriaga & Seljak 1997). The polarization of the CMB photons carries extra physical informations that are not accessible by the study of the temperature anisotropies. Therefore its measurement helps breaking down the degeneracies on cosmological parameters as encounter with temperature anisotropies measurements only (Zaldarriaga et al. 1997). Furthermore, the study of the CMB polarization is also a fundamental tool to estimate the energy scale of inflation which has been proposed to solve the problems of flatness, of isotropy and of the seed perturbations for the formation of the structures in the Universe. Inflationary models predict the presence of tensor perturbations of the metric which will lead to an unique signature in the CMB polarization B modes. The detection of the latter would be a strong proof of such an epoch and also a way to constrain the energy scale at which inflation occurs by measuring the tensor to scalar ratio, r (Turner & White 1996).

Since the beginning of the CMB anisotropies observations with the COsmic Background Explorer (COBE) (Smoot et al. 1992), a great amount of experiments have been designed to determine the CMB tem-

perature angular power spectrum (Netterfield et al. 1997; Miller et al. 1999; deBernardis et al. 2000; Hanany et al. 2000; Lee et al. 2001; Netterfield et al. 2002; Halverson et al. 2002; Sievers et al. 2003; Rubino-Martin et al. 2003; Benoît et al. 2003; Hinshaw et al. 2003; Barkats et al. 2005; Readhead et al. 2004; Leitch et al. 2005; Tristram et al. 2005; Jones et al. 2005). By contrast, the polarization anisotropies, which are between 2 and 5 orders of magnitude weaker than temperature ones are not accurately measured yet. A first detection of the CMB E modes has been performed by DASI (Kovac et al. 2002; Leitch et al. 2005), CAPMAP (Barkats et al. 2005), CBI (Readhead et al. 2004) and more recently by BOOMERANG (Montroy et al. 2005). The TE temperature-polarization cross correlation has been measured by WMAP (Kogut et al. 2003) and BOOMERANG (Piacentini et al. 2005). No detection of the CMB B modes has been reported yet.

The detection of such low signals is possible by improving the instrumental sensitivity, but this is not the only issue in the determination of the CMB polarization power spectra. Other astrophysical emissions as for example the diffuse Galactic emission including free-free, dust and synchrotron and the extragalactic sources emissions also contribute to the sky brightness at the frequencies of interest for CMB studies, and therefore must be efficiently subtracted. These *foregrounds* are particularly important for the study of the CMB polarization. Excluding the free-free emission which is not polarized, the other contributions are ex-

pected to be significantly polarized with similar power on the E and B modes. Recent measurements of the Galactic synchrotron polarization emission at 1.41 GHz (Wolleben et al. 2005) show this emission is significantly polarized at large angular scales. Further, Archeops measurements at 353 GHz show that the Galactic dust diffuse emission is polarized up to a level of 5 to 10 % both in the Galactic center (Benoît et al. 2004) and at high Galactic latitudes (Ponthieu et al. 2005). Finally, for the polarization of extragalactic point sources the sparsity of the data available makes reliable predictions difficult (Tucci et al. 2004; Hildebrand 1996).

A direct subtraction of these foreground contributions on the CMB data will require an accurate knowledge of their spatial distributions and of their electromagnetic spectra. For the synchrotron emission a full sky map at 408 MHz in temperature is available (Haslam et al. 1982) and more recently the WMAP team provided a map at 30 GHz from the MEM decomposition of the first year observations (Bennett et al. 2003b). A fake polarized synchrotron emission template was constructed by (Giardino et al. 2002) based on the Parkes 2400 MHz (Duncan et al. 1997) and Haslam 408 MHz (Haslam et al. 1982) surveys. Furthermore, the electromagnetic spectrum of synchrotron and its spatial distribution are neither accurately known in temperature nor polarization although a first estimate was produced by (Giardino et al. 2002). For the thermal dust emission a full sky map at 100 μm as well as templates for CMB use were extracted from the IRAS and FIRAS data (Schlegel et al. 1999; Finkbeiner et al. 1999). However, neither real nor fake template exists for the dust polarized emission. The dust emission in temperature can be approximated by a grey body of mean temperature 17 K and emissivity between 1.7 and 2.2 (Finkbeiner et al. 1999; Lagache et al. 2003). Currently no measurement on the electromagnetic spectrum of the dust polarized emission is available although we expect it to be the same that for temperature.

To try to overcome the above limitations, a great amount of work has been dedicated to design and implement algorithms for component separation which can discriminate between CMB and foregrounds. These methods can also extract, directly from the CMB data, the emission properties of foregrounds. Wiener filtering has been successfully tested assuming known Gaussian priors for each component and with the electromagnetic spectrum as an input (Tegmark & Efstathiou 1996; Bouchet et al. 2005). Maximum entropy based methods (MEM), assuming entropic priors for the spatial distribution of each of the component, have been intensively used for small sky patches (Hobson et al. 1998) and extended to full sky analysis (Stolyarov et al. 2002). More recently they were adapted to account for spatial anisotropies in the electromagnetic spectra (Stolyarov et al. 2004). More recently, (Eriksen et al. 2005) has developed a new method to perform CMB component separation by parameter estimation and applied it to temperature simulations of the Planck satellite experiments. Independent Component Analysis (ICA) techniques have also been applied to Planck simulations in temperature (Maino et al. 2002) and extended to polarization (Baccigalupi 2004) using the FASTICA algorithm. These methods require no prior on the spectral or spatial distribution of the components but can not make use of the available physical knowledge on the foreground and CMB emissions. In addition, the Spectral Matching Independent Component Analysis (SMICA) (Delabrouille et al. 2003) has been developed to consider both the fully blind analysis for which no prior is assumed and the semi-blind analysis incorporating previous physical knowledge on the astrophysical components. This algorithm, based on the Expectation-Maximization algorithm (EM) (Dempster et al. 1977),

uses the spectral diversity of the components and was developed for temperature only. We present in this paper, PoLEMICA, an extension of this method to polarization including both the blind and semi-blind analysis.

This paper is organized as follows. A simple model of the microwave sky emission in temperature and polarization is described in section 2. Section 3 presents the PoLEMICA MD-MC blind component separation algorithm. Section 4 describe the simulations of the Planck satellite experiment used for testing the algorithm. We present in section 5 the application of the PoLEMICA algorithm to the Planck simulations and discuss its performances. Section 6 discusses the impact of foregrounds in the reconstruction of the temperature and polarization CMB power spectra. We summarize and conclude in section 7.

2 MODEL OF THE MICROWAVE AND SUB-MM SKY

2.1 Multi-detectors Multi-components model

To constrain cosmological models, CMB experiments have to reach an accuracy which is well below the expected level of contamination from astrophysical foregrounds, in temperature and even more critically in polarization. Therefore, an efficient separation between CMB and foregrounds is crucial for the success of future polarization experiments. To perform such a separation, the diversity of the electromagnetic spectra and of the spatial spectra of the components is generally used. Observations from a multi-band instrument can be modeled as a linear combination of multiple physical components leading to what is called a Multi-Detectors Multi-Components (MD-MC) modeling.

Assuming an experiment with n_v detector-bands at frequencies ν_i and n_c physical components in the data, for each Stokes parameter (I , Q and U) and for each pixel on the sky map we can write

$$y^v(\mathbf{r}) = A_c^v \cdot s^c(\mathbf{r}) + n^v(\mathbf{r}) \quad (1)$$

where $s^c(\mathbf{r})$ is the map of the c component, $n^v(\mathbf{r})$ refers to the noise map for each ν_i band and A_c^v which is called the *mixing matrix*, gives the electromagnetic spectrum behavior for the component c and frequency ν_i . Beam smoothing and filtering effects are not considered in this work.

As in the temperature case, it is more convenient to work in spherical harmonics space, where equation (1) can be rewritten independently for each $\{\ell, m\}$ assuming a full sky coverage. Thus equation (1) reads for $X = \{T, E, B\}$ and for each frequency band and for each $\{\ell, m\}$

$$y_{\ell m}^{v, X} = \sum_{c=1}^{n_c} A_c^{v, X} s_{\ell m}^{c, X} + n_{\ell m}^{v, X} \quad (2)$$

where $y_{\ell m}^{v, X}$ is a vector of size $(3 \cdot n_v \cdot n_\ell \cdot n_m)$, $s_{\ell m}^{c, X}$ is a $(3 \cdot n_c \cdot n_\ell \cdot n_m)$ vector and $n_{\ell m}^{v, X}$ is a vector of the same size than $y_{\ell m}^{v, X}$. $A_c^{v, X}$ is a matrix of $(3 \cdot n_v) \times (3 \cdot n_c)$ elements formed from the mixing matrix of each of the modes, T , E and B .

The aim of the component separation algorithm presented in this paper is to extract $A_c^{v, X}$, $s_{\ell m}^{c, X}$ and $n_{\ell m}^{v, X}$ from the $y_{\ell m}^{v, X}$ sky observations.

2.2 Simulated microwave and sub-mm sky

Following the MD-MC model discussed above and given an observational setup, we construct, using the HEALPix pixelization

scheme (Górski et al. 1999) and in CMB temperature units, fake I , Q and U maps of the sky at each of the instrumental frequency bands. For these maps we consider three main physical components in the sky emission: CMB, thermal dust and synchrotron. Instrumental noise is modeled as white noise.

CMB

The CMB component map is randomly generated from the polarized CMB angular power spectra computed with the CAMB software (Lewis et al. 2000) for a set of given cosmological parameters. In the following we have used $H_0 = 71 \text{ km} \cdot \text{s}^{-1} \cdot \text{Mpc}^{-1}$, $\Omega_b = 0.044$, $\Omega_m = 0.27$, $\Omega_\Lambda = 0.73$ and $\tau = 0.17$ that are the values of the cosmological concordance model according to the WMAP results (Spergel et al. 2003). Two set of simulations are performed with tensor-to-scalar ratio r of 0.7. The latter corresponds to the upper limit obtained with the WMAP satellite (Spergel et al. 2003). We also consider gravitational lensing effects as described in (Hu 2000; Challinor & Chon 2002; Okamoto & Hu 2003).

Synchrotron

For the diffuse Galactic synchrotron emission we use the template maps in temperature and in polarization provided by (Giardino et al. 2002). These template maps were derived in temperature directly from the Haslam map at 408 MHz (Haslam et al. 1982). The polarization maps in Q and U were constructed from the intensity map from a constrained realization of the polarization angles using the Parkes 2400 MHz survey (Duncan et al. 1997). A template of the spatial variations of the synchrotron spectral index is also provided by (Giardino et al. 2002). Here we have chosen to use a constant spectral index equal to the mean of the spectral index map, $\alpha = -2.77$, so that the simple linear model of the data holds. A more realistic treatment of the synchrotron emission will require a specific model of the spectral index spatial variations in order to ensure separability between components.

Dust

In the case of the thermal dust we dispose of few observational data of the polarized diffuse emission and to date no template for this is available. Thus, we have considered a power-law model from (Prunet et al. 1998) to describe the angular power spectra in temperature and in polarization. We have renormalized this model to mimic at large angular scales the TE cross power spectrum measured by Archeops at 353 GHz (Ponthieu et al. 2005). The rms of the final dust map is probably overestimated as we do not account for the variation of the dust emission with respect to Galactic latitude. The power spectra models are computed at 100 GHz in μK_{RJ} units. I , Q and U full-sky maps are generated randomly from these power spectra. We extrapolate them to each of the frequency of interest by assuming a grey body with an emissivity of 2. Finally, the μK_{RJ} maps are converted into μK_{CMB} units.

Noise

Noise maps for each channel are generated from white noise realizations normalized to the nominal level of instrumental noise for that channel.

ν (GHz)	30	40	70	100	143	217	353
CMB	1.0	1.0	1.0	1.0	1.0	1.0	1.0
Sync.	1.0	0.46	0.11	0.045	0.021	0.012	0.014
Dust	0.0006	0.001	0.003	0.008	0.021	0.088	1.0
Noise I	4.12	4.03	4.06	1.47	1.0	1.47	4.54
Noise P	2.91	2.95	2.98	1.51	1.0	1.51	4.59

Table 1. Electromagnetic spectrum, in arbitrary units, of the CMB, dust and synchrotron components at each of the Planck channels. Relative noise levels in the temperature and in the polarization maps taking as reference the 143 GHz channel are also displayed.

The electromagnetic spectra, in arbitrary units, for the CMB, dust and synchrotron emissions are displayed in table 1 (these are the values used in the mixing matrix A) for the Planck satellite simulations presented in section 4. We also present the relative noise level taking as reference the 143 GHz channel. The noise levels used at 143 GHz are $6.3 \mu\text{K}_{\text{CMB}}$ (in temperature) and $12.3 \mu\text{K}_{\text{CMB}}$ (in polarization) per square pixels of side 7 arcmin and for a 14-months Planck mission (Planck Consortium 2005).

3 A MD-MC COMPONENT SEPARATION METHOD FOR POLARIZATION

3.1 MD-MC model for the temperature and polarization power spectra.

To reduce the number of unknown parameters in the model described by equation (2), it is interesting to rewrite this equation in terms of the temperature and polarization auto and cross power spectra. This will considerably reduce the computing time with no loss of information.

We define the density matrices associated with the data, y , the physical components, s and the noise, n , as follows

$$R_\chi(\ell) \equiv \langle \chi_{\ell m}^{i, X} \cdot \chi_{\ell m}^{i', X' \dagger} \rangle, \quad \chi = \{y, s, n\} \\ = \frac{1}{2\ell + 1} \sum_{l=-m}^m \chi_{\ell m}^{i, X} \cdot \chi_{\ell m}^{i', X' \dagger} \quad (3)$$

where i represents frequency, ν , for the data and noise matrices and component, c , for the physical-components matrix. Averaging over bins on ℓ we obtain

$$R_\chi(b) \equiv \frac{1}{n_b} \sum_{\ell \in \mathcal{D}_b} \langle \chi_{\ell m}^{i, X} \cdot \chi_{\ell m}^{i', X' \dagger} \rangle \quad (4)$$

where \mathcal{D}_b is the set of ℓ values which contributes to bin b and n_b is the number of such multipoles. In the following, N_b , represents the total number of bins used in the analysis.

For each bin b , equation (2) reads

$$R_y(b) = AR_s(b)A^T + R_n(b) \quad (5)$$

where $R_y(b)$ and $R_n(b)$ are $(n_\nu \cdot 3) \times (n_\nu \cdot 3)$ matrices and $R_s(b)$ is a $(n_c \cdot 3) \times (n_c \cdot 3)$ matrix.

To fully understand the component separation algorithm described below it is interesting to have a closer look to the content of the three density matrices defined above (see appendix for a concrete example).

$R_y(b)$ represents the input density matrix computed from the observed multi-band data. This matrix is composed of 3×3 symmetric blocks each of them containing in the diagonal the auto-power spectra, TT , EE , BB and in the off-diagonal the cross-power

spectra TE , EB and TB . A single block represents either the auto-correlation of a single channel (for diagonal blocks) or the cross-correlation between two channels (for off-diagonal blocks).

Assuming that the physical components in the data are statistically independent and uncorrelated makes the $R_s(b)$ a $3 \cdot n_c \times 3 \cdot n_c$ block diagonal matrix. As above each block, corresponding to the c^{th} physical component, contains in the diagonal the auto-power spectra, TT , EE , BB and in the off-diagonal the cross-power spectra TE , EB and TB .

We also assume that the noise is uncorrelated between channels and therefore, $R_n(b)$ is a diagonal matrix containing the noise auto power spectra TT , EE and BB for each of the channels.

3.2 Spectral matching algorithm

From equation (5) we observe that, for each bin b , the data density matrix $R_y(b)$, of size $9 \times n_y^2$, is fully defined by the set of parameters $\theta(b) = \{A, R_s(b), \text{diag}(R_n(b))\}$ which corresponds to a total of $3 \times n_y \times n_c + 6 \times n_c + 3 \times n_y$ parameters. This indicates that from the CMB data set and under the hypothesis presented above it is possible to simultaneously estimate the mixing matrix, the physical component's temperature and polarization power spectra and the noise's temperature and polarization power spectra for each of the channels. Further, assuming white noise in the maps only three noise parameters per channel (for TT , EE and BB) need to be estimated for the entire range in ℓ . This reduces the overall set of parameters to $3 \times n_y \times n_c + 6 \times n_c \times N_b + 3 \times n_y$ where N_b is the number of bins.

The likelihood function

To estimate the above parameters from the data we have extended to the case of polarized data the spectral matching algorithm developed by (Delabrouille et al. 2003) for temperature only. The key issue of this method is to estimate these parameters, or some of them (for a semi-blind analysis), by finding the best match between the model density matrix, $R_y(b)$, computed for $\theta(b)$ and the data density matrix $\tilde{R}_y(b)$ obtained from the multi-channel data. Assuming that the different physical components and the noise are realizations of Gaussian stationary fields (Wittle approximation), the log-likelihood function of the form

$$-\mathcal{L} = \sum_{b=1}^{N_b} n_b \left[\text{Tr} \left(\tilde{R}_y(b) R_y^{-1}(b) \right) + \log \det \left(R_y(b) \right) \right] + c. \quad (6)$$

is a reasonable measure of the mismatch between data and model.

EM algorithm

The maximization of the likelihood function is achieved via the Expectation-Maximization algorithm (EM) (Dempster et al. 1977). This algorithm will process iteratively from an initial value of the parameters $\theta_0(b)$ following a sequence of parameter updates $\theta_i(b)$, called 'EM steps'. During the i^{th} E-step we compute the expectation value for the likelihood from the $(i-1)^{\text{th}}$ iteration's parameters. The i^{th} M-step maximizes the likelihood (i.e. minimizes the log-likelihood) to compute the i^{th} set of parameters. By construction each EM step improves the spectral fit by maximizing the likelihood. For a more detailed review of the spectral matching EM algorithm used here, see (Snoussi et al. 2001) and

(Delabrouille et al. 2003) and appendix A for the formalism used to describe the polarized sky model and data.

In the MD-MC model presented above there is a scale indetermination on the value of A and R_s and only the product AR_sA^T is scale invariant. Thus, to ease the convergence of the algorithm, we renormalize each column of A to unity at each EM iteration and correct the R_s density matrix accordingly so that the product AR_sA^T is unchanged.

Initialization of the algorithm

To start-up the EM algorithm the parameters of the fit, θ , need to be initialized to reasonable values to avoid exploring local maxima in the likelihood function.

In the case of the mixing matrix, A , we can consider, in a first approximation, that the electromagnetic spectrum is the same in temperature and polarization for each of the components. Therefore, we can concentrate on guessing the electromagnetic spectrum in the temperature data where we expect the signal to noise to be larger. When no physical prior is available this can be obtained by using the n_c dominant eigenvectors of the data density matrix for temperature only, \tilde{R}_y^{TT} . Each of them represent the change of power with frequency for the dominant components in the data. Notice that these components and the physical ones are not necessarily the same. On one hand, we can have in the data extra components which have not been identified as for example residual systematics. On the other hand, the electromagnetic spectrum of the physical components may present spatial variations as it is, for example, the case for the Galactic synchrotron diffuse emission. In the following, we will consider that the data contain only identified physical components with spatially constant electromagnetic spectrum. If this is not the case, a careful preanalysis of the initialization parameters is needed and this is not discussed in this paper.

Assuming the mixing matrix previously initialized, the physical-components density matrix can be obtained from a noiseless fit to the data as follows

$$R_{s,0}(b) = \text{blockdiag} \left(\left(A_0^T A_0 \right)^{-1} A_0^T \tilde{R}_y(b) A_0 \left(A_0 A_0^T \right)^{-1} \right) \quad (7)$$

Finally, from A_0 and $R_{s,0}(b)$ the noise density matrix is given by

$$R_{n,0}(b) = \text{diag} \left(\sum_b \frac{n_b}{n} \left(\tilde{R}_y(b) - A_0 R_{s,0} A_0^T \right) \right) \quad (8)$$

where $n = \sum n_b$. Here we implicitly assume that the noise is white and not correlated between different channels.

4 SIMULATED OBSERVATIONS

We have performed various sets of simulations of the expected Planck satellite data to intensively test the algorithm presented above. For each of those, we performed 300 realizations considering full-sky maps containing either instrumental noise, CMB, dust and synchrotron or instrumental noise and CMB. We simulate maps at the LFI and HFI polarized channels, 30, 40 and 70 GHz for LFI and 100, 143, 217 and 353 GHz for HFI. These maps are in HEALPix pixelization (Górski et al. 1999) and correspond to a 14-month survey.

(i) [planck a]: We simulate maps at $n_{\text{side}} = 512$ (pixels of area $\sim 47 \text{ arcmin}^2$). We include in the simulations CMB emission assuming tensor to scalar ratios of 0.7 and 0.1 and gravitational

lensing. The simulations also contain synchrotron and thermal dust emissions as described in section 2. This n_{side} permits the reconstruction of the angular power spectra up to $\ell \simeq 1500$. The reconstructed spectra will be averaged over bins of size 20 in ℓ . With these simulations we test the separation method at small angular scales.

(ii) [planck b]: We simulate maps at $n_{\text{side}} = 128$ (pixels of area $\sim 755 \text{ arcmin}^2$) for CMB only. This n_{side} permits the reconstruction of the power spectra up to $\ell \simeq 400$. This maximum ℓ value is enough to study the effect of gravitational waves in the BB spectrum which is maximum around $\ell = 100$ for the concordance model. The reconstructed spectra are averaged over bins of size 10 in ℓ . These simulations were performed for fast and intense test of the algorithm in the easiest possible case.

(iii) [planck c]: We simulate maps at $n_{\text{side}} = 128$ including CMB, thermal dust and synchrotron emissions. The reconstructed spectra are averaged over bins of size 10 in ℓ . These simulations were performed to check the impact of foregrounds in the reconstruction of the CMB power spectra.

5 TESTING AND PERFORMANCES

We have applied the MD-MC POLEMICA component separation algorithm to the simulations presented above. For each set of simulations we have computed the data density matrix $R_y(b)$ and applied the algorithm with different degrees of freedom:

(i) First, we assume that the mixing matrix, A , is known. We construct the A matrix from the exact electromagnetic spectrum of each of the components and fix it in the algorithm. Therefore, we take as parameters for the fit $\theta(b) = \{R_s(b), \text{diag}(R_n(b))\}$ for each bin b . With this test we want to check the spatial separability of the components. In the following, we refer to this type of component separation as *A-fixed* separation.

(ii) Secondly, we have performed what we call a *CMB semi-blind* separation. The A matrix is fitted as well as R_s and R_n , but assuming a prior on the CMB electromagnetic spectrum. Thus, the columns of the A matrix corresponding to the CMB are fixed to unity and the set of parameters for the fit is $\theta(b) = \{A_{i,j \neq \text{CMB}}, R_s(b), \text{diag}(R_n(b))\}$ for each bin b . The initialization of A , except for the CMB, is performed as described in section 3.2. This kind of prior in the CMB electromagnetic spectrum is a reasonable approximation because the former is well-known.

(iii) Finally we have performed a *blind* separation fitting all the parameters $\theta(b) = \{A, R_s(b), \text{diag}(R_n(b))\}$ for each bin b including the CMB electromagnetic spectrum.

We have performed these three types of analysis in all the simulated sets. To ensure the reliability of the results we performed 10000 EM iterations and checked, for each simulation, the convergence of the EM algorithm. In the following we present the main results obtained in reverse order going from (iii) to (i) and if not stated otherwise we assume white noise $R_n(b) = \sigma_{TT,EE,BB}^2$

5.1 Blind separation analysis

We present here a *blind* analysis of the [planck c] simulations for which we assume three physical components in the data: CMB and Galactic dust and synchrotron emissions. The noise and physical-components density matrices as well as the mixing matrix are initialized as described in section 3.2. No physical priors are assumed neither for synchrotron nor dust. For CMB, if not stated

otherwise, we initialize the electromagnetic spectrum to 1 for temperature and polarization. This is a reasonable approximation as we expect the Planck data to be calibrated to better than 1 % (Planck Consortium 2005).

Reconstruction of the power spectra

Figure 1 shows the *blind* reconstructed CMB temperature and polarization power spectra, in μK_{CMB}^2 , for the 100 GHz channel (crosses). The input model is overplotted in blue. The mean and the error bars are computed from the analysis of 300 simulations.

We observe that C_ℓ^{TE} , C_ℓ^{TB} and C_ℓ^{EB} are recovered with no bias, up to $\ell = 383$, which is the largest accessible ℓ value at $n_{\text{side}} = 128$. In the same way, C_ℓ^{EE} is accurately reconstructed except for the very high ℓ values for which pixelization problems may appear (see section 6.1). We also reconstruct efficiently C_ℓ^{TT} although a small bias (below 10 %) is introduced at low ℓ mainly due to confusion with the synchrotron emission as discussed in the following. The C_ℓ^{BB} spectrum is not recovered at all and a significant bias is observed. This bias, due mainly to statistical residual noise as discussed in the following section, depends only on the signal to noise ratio and does not affect the reconstruction of the other components.

Figure 2 shows the reconstructed thermal dust emission power spectra, C_ℓ^{TT} , C_ℓ^{EE} , C_ℓ^{BB} , C_ℓ^{TE} , C_ℓ^{TB} and C_ℓ^{EB} , in μK_{CMB}^2 , at 353 GHz. For comparison we overplot in red the input model. The mean and the error bars displayed were computed using a total of 300 simulations. The reconstruction is fully efficient for C_ℓ^{TT} , C_ℓ^{EE} , C_ℓ^{TB} and C_ℓ^{EB} up to $\ell = 383$. The C_ℓ^{EE} and C_ℓ^{BB} are accurately reconstructed except at $\ell > 350$ where a small bias (below 10 %) appears. The TB and EB spectra are compatible with zero as expected from the input model. These results are consistent with the fact that the simulated thermal dust emission dominate the simulated maps at the LFI channels for which the signal to noise ratio is larger.

Finally, we present in figure 3 the *blind* reconstructed synchrotron power spectra, in μK_{CMB}^2 , at 30 GHz. We overplot in green the power spectrum of the input temperature and polarization synchrotron map from (Giardino et al. 2002). Here again C_ℓ^{EE} , C_ℓ^{BB} , C_ℓ^{TE} , C_ℓ^{TB} and C_ℓ^{EB} are recovered efficiently. A bias at low ℓ (below 20 %) is observed for C_ℓ^{TT} . This is due, as discussed in the following, to the slight mixing-up of the synchrotron and CMB emissions in temperature.

Reconstruction of the mixing matrix

The slight mixing up between synchrotron and CMB is better observed in the reconstructed mixing matrix. The first row of figure 4 shows the *blind* recovered A matrix for dust, synchrotron and CMB in the case of the [planck c] simulations. The electromagnetic spectrum for T , E and B are respectively traced in green, red and blue. For comparison we overplot the input electromagnetic spectrum for each of the components (black dashed line). For convenience we have renormalized the electromagnetic spectrum so that it is unity at 353 GHz, 30 GHz and 100 GHz for dust, synchrotron and CMB respectively. It is important to remark that the reconstruction of the electromagnetic spectra for temperature and polarization is performed independently. We observe that the error bars are larger for polarization than for temperature as we would expect from the smaller signal to noise ratio in polarization.

The dust electromagnetic spectrum is reconstructed with no bias both in temperature and polarization even at the lowest LFI frequency channels. Furthermore, the reconstructed synchrotron electromagnetic spectra in polarization are not biased. In temperature

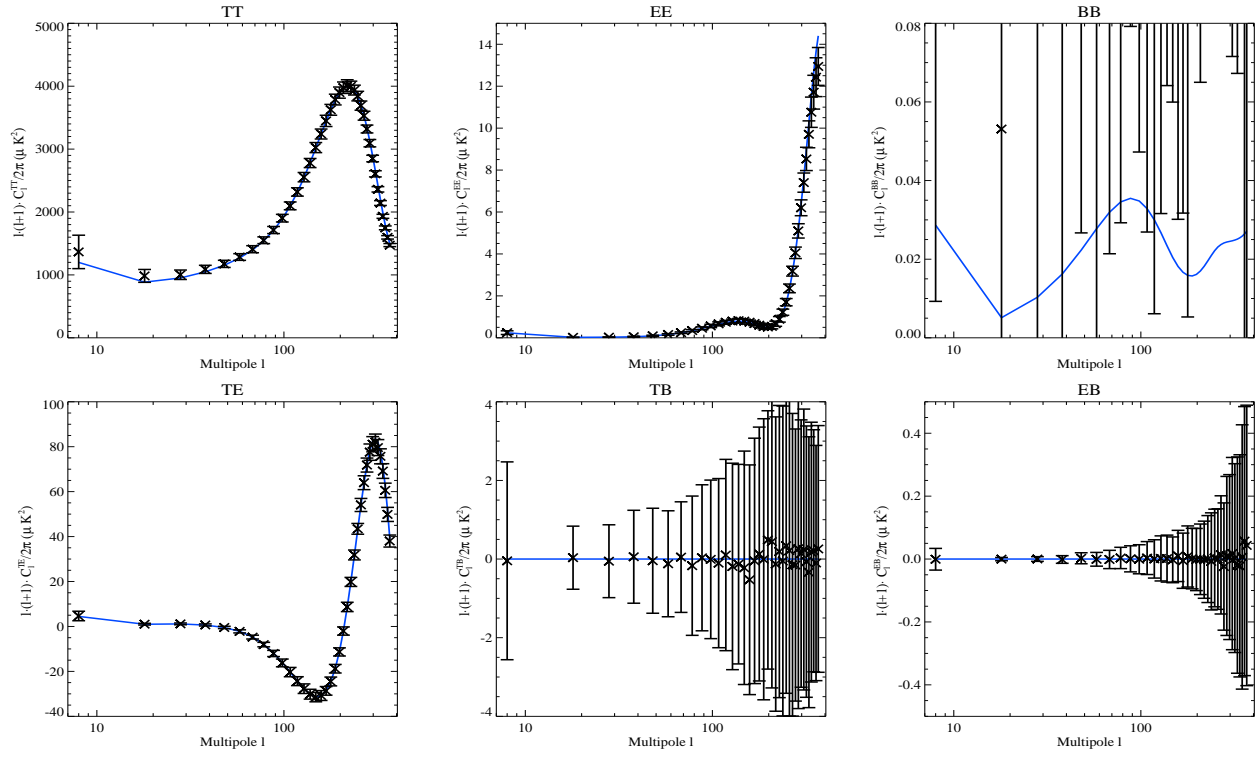


Figure 1. *Blind* reconstructed CMB power spectra (crosses), C_ℓ^{TT} , C_ℓ^{EE} , C_ℓ^{BB} , C_ℓ^{TE} , C_ℓ^{TB} and C_ℓ^{EB} , in $\mu\text{K}_{\text{CMB}}^2$, at 100 GHz for the [planck c] simulations. We overplot in blue the input model. Error bars are computed using a total of 300 simulations.

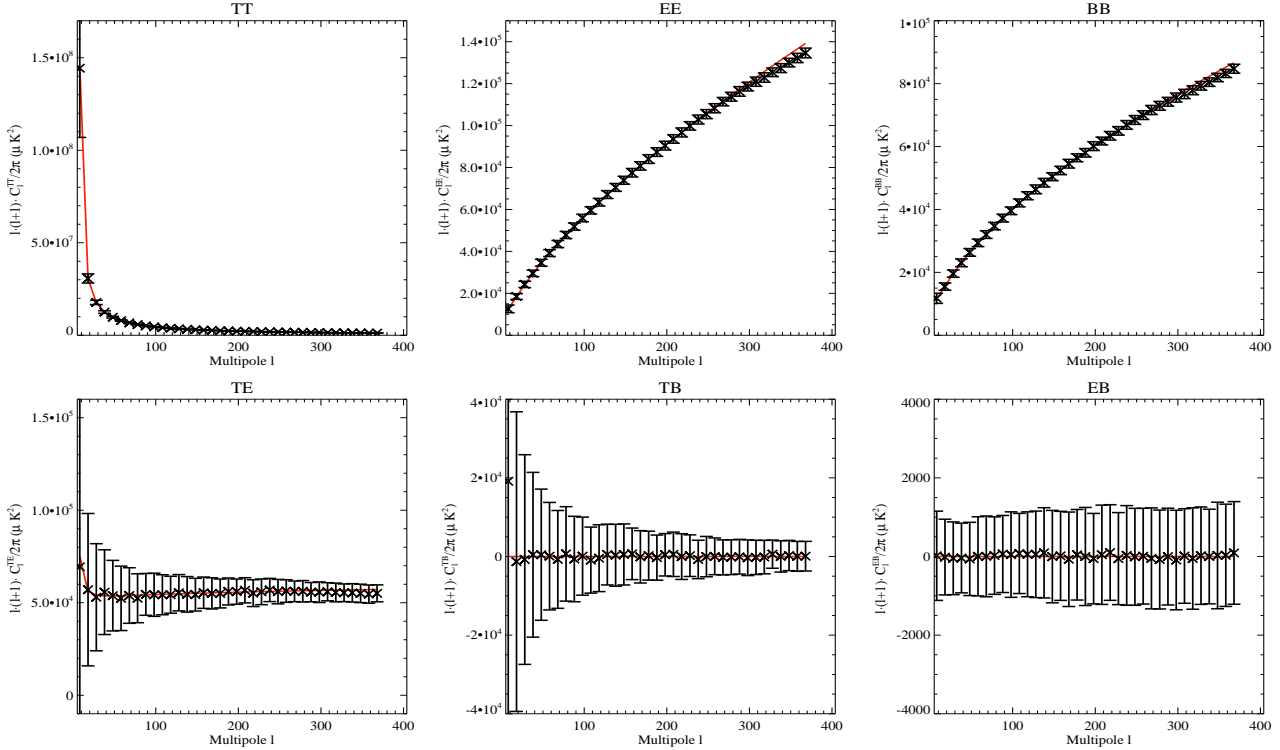


Figure 2. *Blind* reconstructed thermal dust emission power spectra, C_ℓ^{TT} , C_ℓ^{EE} , C_ℓ^{BB} , C_ℓ^{TE} , C_ℓ^{TB} and C_ℓ^{EB} , in $\mu\text{K}_{\text{CMB}}^2$, at 353 GHz for the [planck c] simulations. We overplot in red the input model. Error bars are computed using a total of 300 simulations.

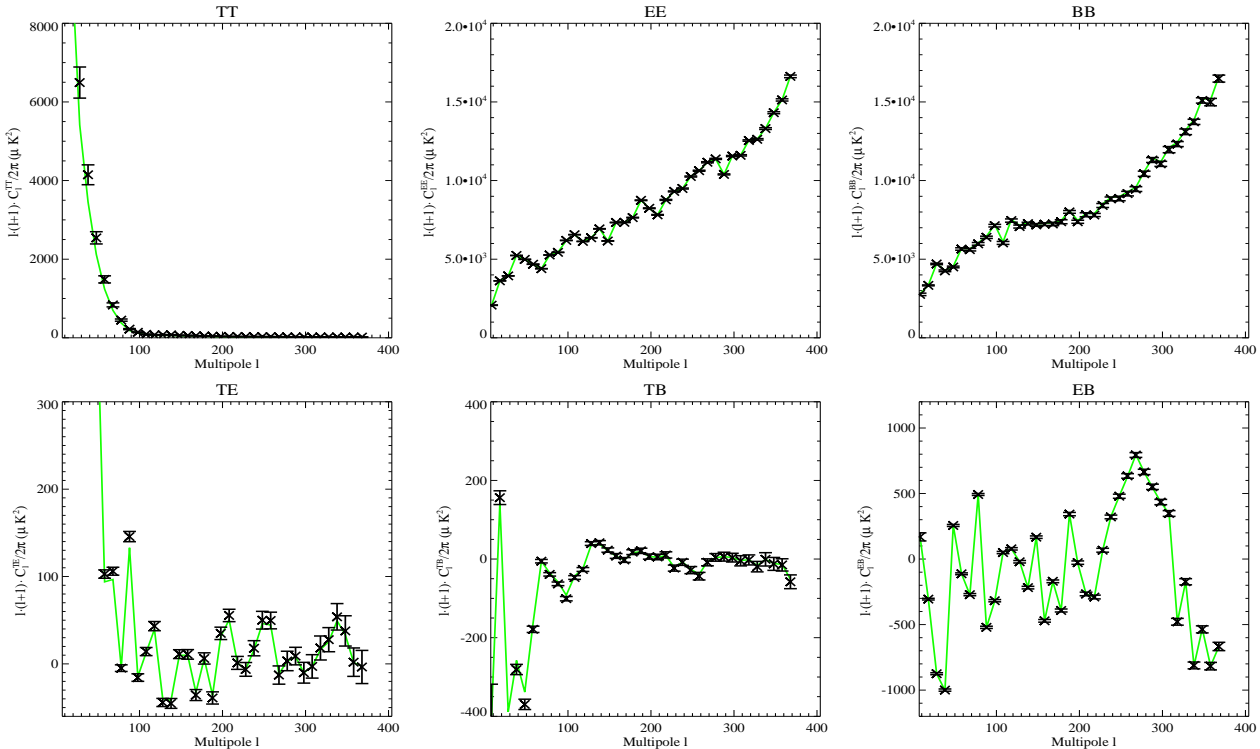


Figure 3. Blind reconstructed synchrotron emission power spectra, C_{ℓ}^{TT} , C_{ℓ}^{EE} , C_{ℓ}^{BB} , C_{ℓ}^{TE} , C_{ℓ}^{TB} and C_{ℓ}^{EB} , in μK_{CMB}^2 , at 353 GHz. We overplot in green the input model. The error bars are computed using 300 simulations. These are significantly smaller than for the other two components because they do not include cosmic variance. Indeed we use the same synchrotron temperature and polarization maps for all the simulations.

we observe that the spectrum flattens out at intermediate frequencies between 70 and 217 GHz. This is the cause of the slight mixing up between synchrotron and CMB. This mixing up does not happen in polarization for which the synchrotron emission dominates over the CMB emission. Finally, the reconstruction of the CMB electromagnetic spectrum from the T and E modes, although noisy for the latter, is not biased. However for the B modes the reconstruction is very poor because of the very low signal to noise ratio (below 10^{-2} for $\ell > 100$).

We have repeated the analysis with no prior in the electromagnetic spectrum of the CMB. We use instead the eigenvector corresponding to the third larger eigenvalue of the data density matrix. The results for dust and synchrotron remain unchanged. For CMB the electromagnetic spectrum at 30 and 353 GHz is not reconstructed neither in temperature nor in polarization and the results for B are significantly degraded at all frequencies. However, the results on the reconstruction of the spatial power spectra remain unchanged for all the physical components including CMB. This can be easily understood as the reconstruction of the CMB power spectra is mainly dominated by the intermediate frequency maps, from 70 to 217 GHz, where the A matrix is accurately reconstructed.

Assuming equal temperature and polarization electromagnetic spectrum

In the previous analysis we have computed the electromagnetic spectrum of the physical components independently for each mode T , E and B . In a more realistic approach we should consider a single electromagnetic spectrum for the polarization E and B modes

which may be different from the temperature one. We have repeated the analysis under the above hypothesis and the results remain roughly the same with respect to the reconstruction of the spatial power spectra and of the electromagnetic spectrum. For synchrotron and dust the E and B modes have roughly the same power in our simulations and therefore we expect only variations in the error bars. For CMB the E mode largely dominates the B mode and therefore we expect no significant contribution from the latter to the electromagnetic spectrum reconstruction.

The differences between the temperature and polarization electromagnetic spectra are expected to be small for dust and synchrotron (Planck Consortium 2005) and none for the CMB (Zaldarriaga & Seljak 1997). Therefore, in the case of a perfectly calibrated experiment, we can consider, in a first approximation, that the polarization and the temperature electromagnetic spectra are the same. The *blind* analysis of the [planck c] simulations under this hypothesis shows no evidence of mixing up between synchrotron and CMB. This can be clearly observed in the second row of figure 4 where we represent from left to right the reconstructed electromagnetic spectrum of the dust, synchrotron and CMB emissions respectively. No bias is observed for any of the physical components including synchrotron for which the flatten out of the spectrum observed before is not present.

Figures 5 and 6 show the CMB and synchrotron reconstructed spatial power spectra in temperature and polarization. We do not observe a bias neither on the synchrotron nor on the CMB TT power spectra. Furthermore, we observe that the CMB BB modes, although biased at large ℓ values, are fairly reconstructed up to $\ell = 60$. For the other modes, the results are similar to those presented in the previous section.

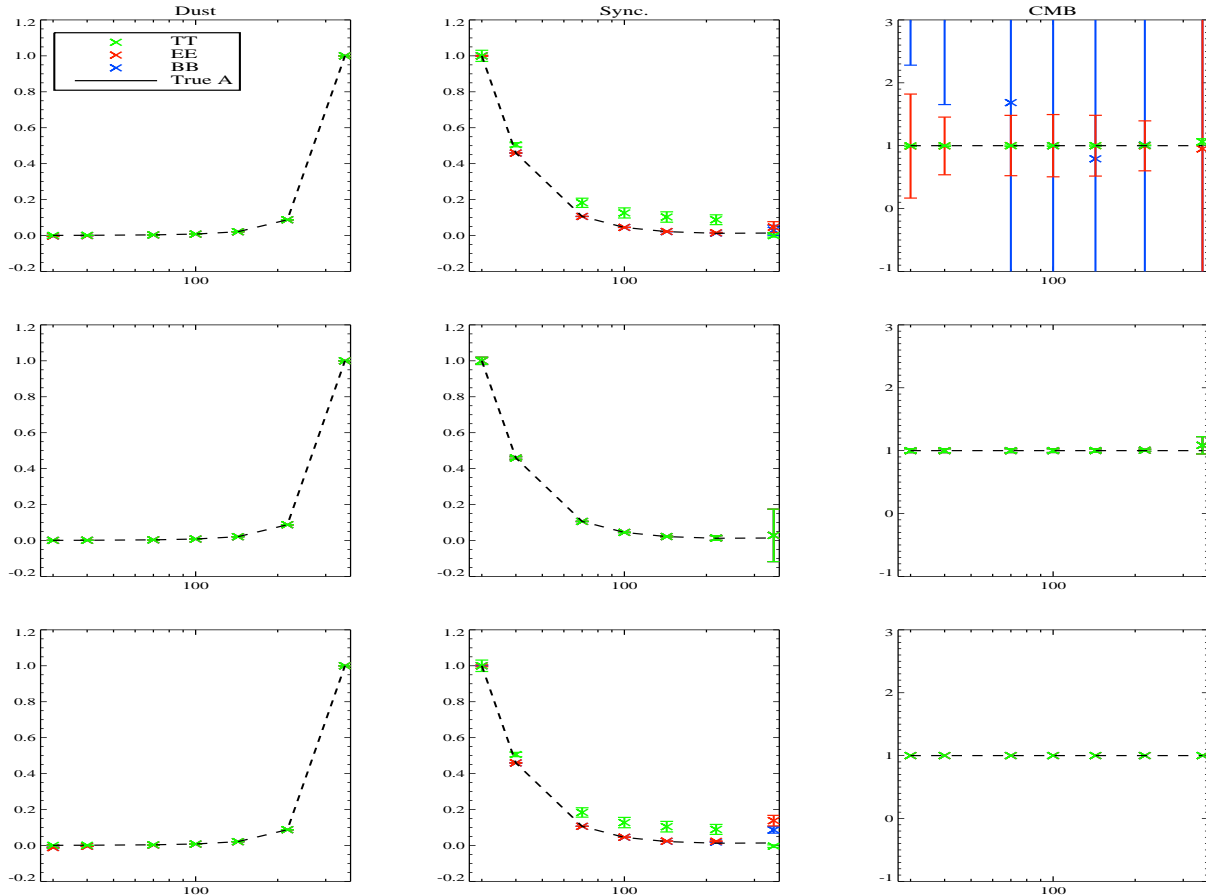


Figure 4. Reconstructed mixing matrix, A . Columns, from left to right, correspond to the reconstructed A matrix for dust, synchrotron and CMB respectively. Rows, from top to bottom, correspond to the *blind*, *blind* assuming equal temperature and polarization electromagnetic spectrum and the *CMB semi-blind* analysis of the [planck c] simulations. We display the output electromagnetic spectrum computed for the T (green), E (red) and B (blue) modes as well as the input electromagnetic spectrum (dashed black).

5.2 Semi-blind separation

The separation method allows us to easily include previous knowledge on the physical components either as priors or as facts. In the previous section we considered a prior on the CMB emission. In the following we move a step forward in the analysis assuming the CMB electromagnetic spectrum known and performing what we call a *CMB semi-blind* analysis. For this analysis, the columns of the mixing matrix corresponding to the CMB are initialized to the CMB electromagnetic spectrum and are not updated by the algorithm. For the other components we consider independent electromagnetic spectra for temperature and polarization and they are initialized as for the *blind* analysis.

The third row of figure 4 shows the reconstructed mixing matrix for the *CMB semi-blind* analysis considering the [planck c] simulations. The results are similar to those of the *blind* analysis discussed before. The dust electromagnetic spectrum is accurately recovered in temperature and polarization. For synchrotron, the polarization spectrum is accurately recovered but the temperature one flattens out at intermediate frequencies with respect to the input model. Therefore, the reconstructed dust and synchrotron spatial power spectra in temperature and polarization are similar to those of the *blind* analysis. The dust power spectra are accurately reconstructed in temperature and polarization. For synchrotron the power spectra are also accurately reconstructed except for the TT mode

which present a slight bias (below 20%) at large angular scales ($\ell < 60$). In general the error bars are smaller for the *CMB semi-blind* analysis as discussed in section 6.3.

The reconstructed CMB power spectra for the *CMB semi-blind* analysis are represented in black on figure 7. All of them are accurately reconstructed with no bias except for the BB mode. For the latter the reconstruction is accurate up to $\ell = 60$ and there is bias. This bias is due to residual noise and is not related to the uncertainties on the reconstruction of the electromagnetic spectrum for the other physical components. To check this we have also performed a *A-fixed* analysis assuming the electromagnetic spectrum of all physical components known. The results of this analysis are overplotted in red on the figure. We observe that reconstruction is equivalent to that of the *CMB semi-blind* analysis but for the error bars which are smaller as described in section 6.3. This indicates that the bias in the BB mode is mainly due to residual noise as discussed in section 6.2.

6 DISCUSSIONS

6.1 Reconstruction of the small angular scales

In the previous section we have fully described the analysis of the [planck c] simulations at $n_{\text{side}} = 128$ for which the reconstruc-

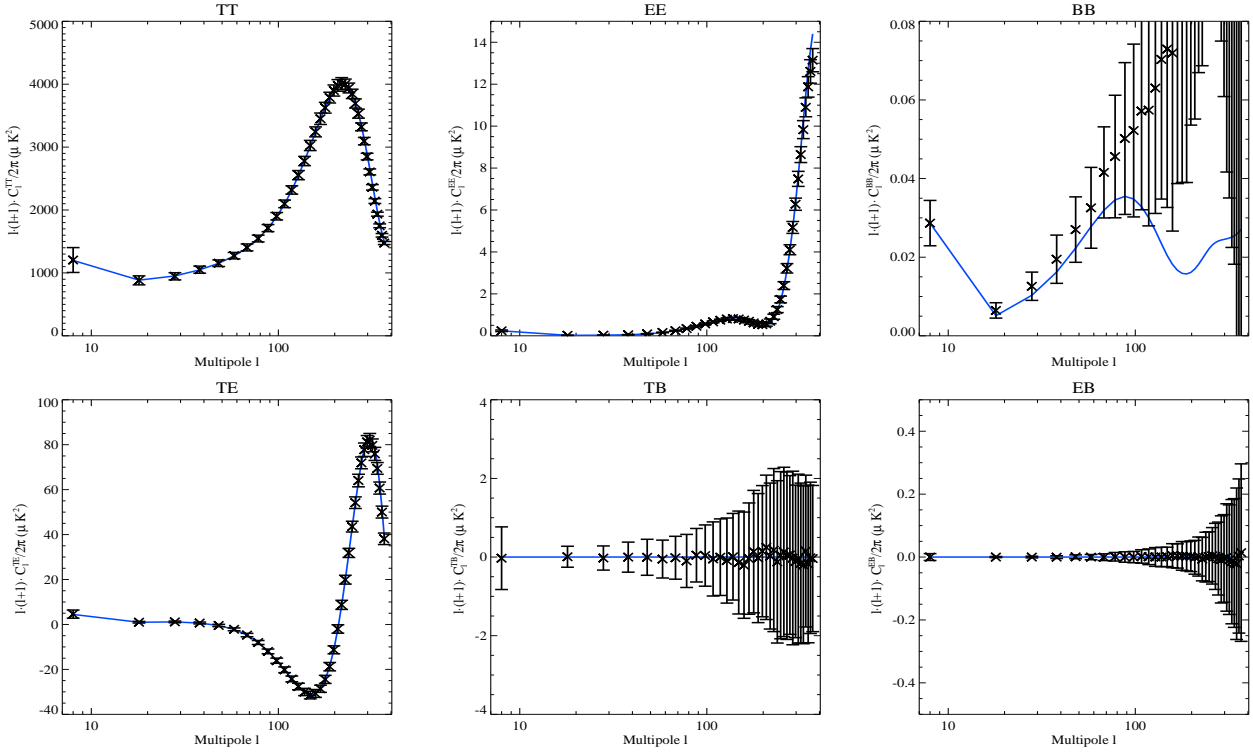


Figure 5. Same as figure 1 except for a *blind* analysis assuming equal temperature and polarization electromagnetic spectrum.

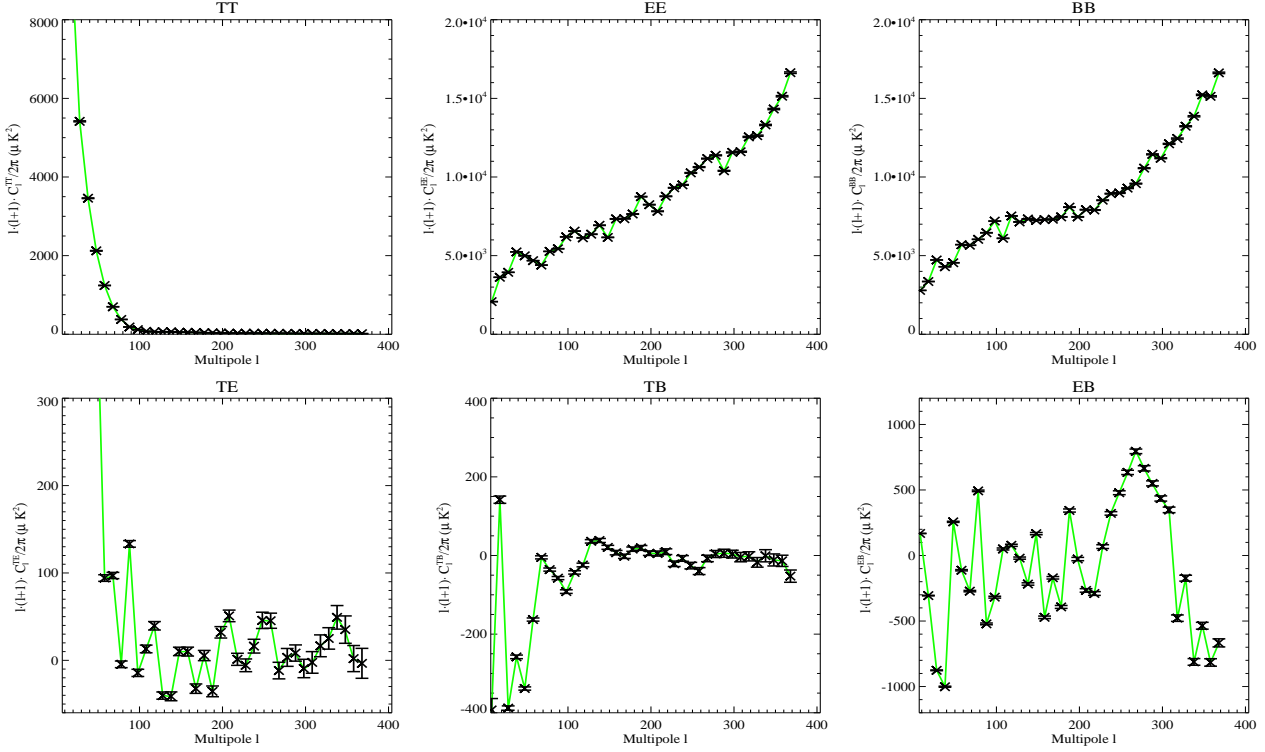


Figure 6. Same as figure 3 but for a *blind* analysis assuming equal temperature and polarization electromagnetic spectrum.

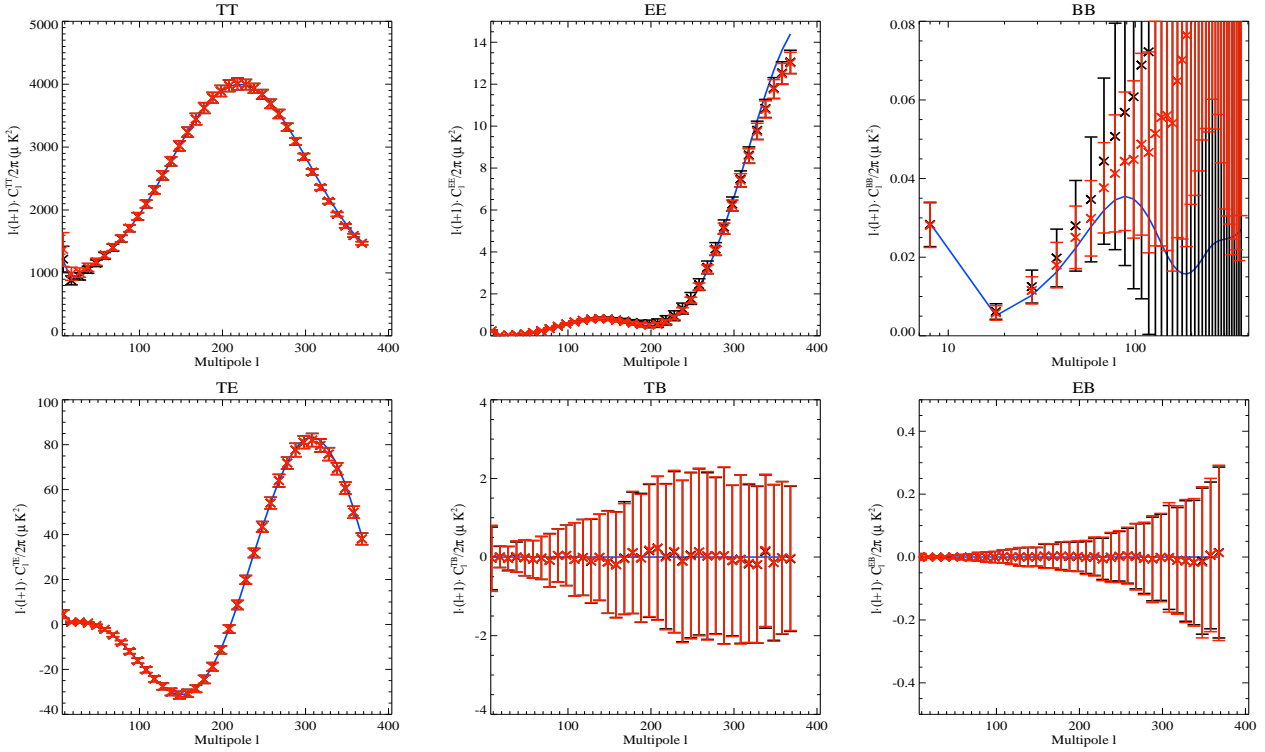


Figure 7. Same as figure 1 but for a CMB *semi-blind* (black) and *A-fixed* (red) analysis (see text for details).

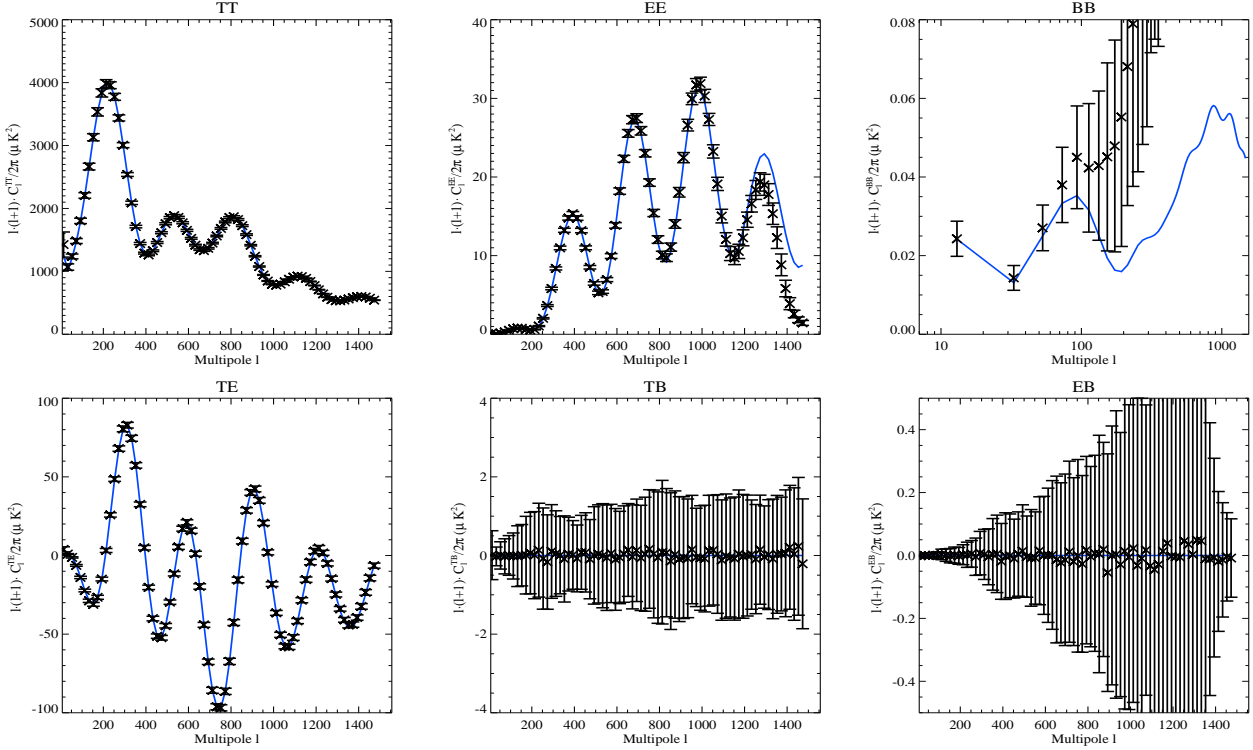


Figure 8. Same as figure 1 but for the [planck a] simulations for a CMB *semi-blind* analysis.

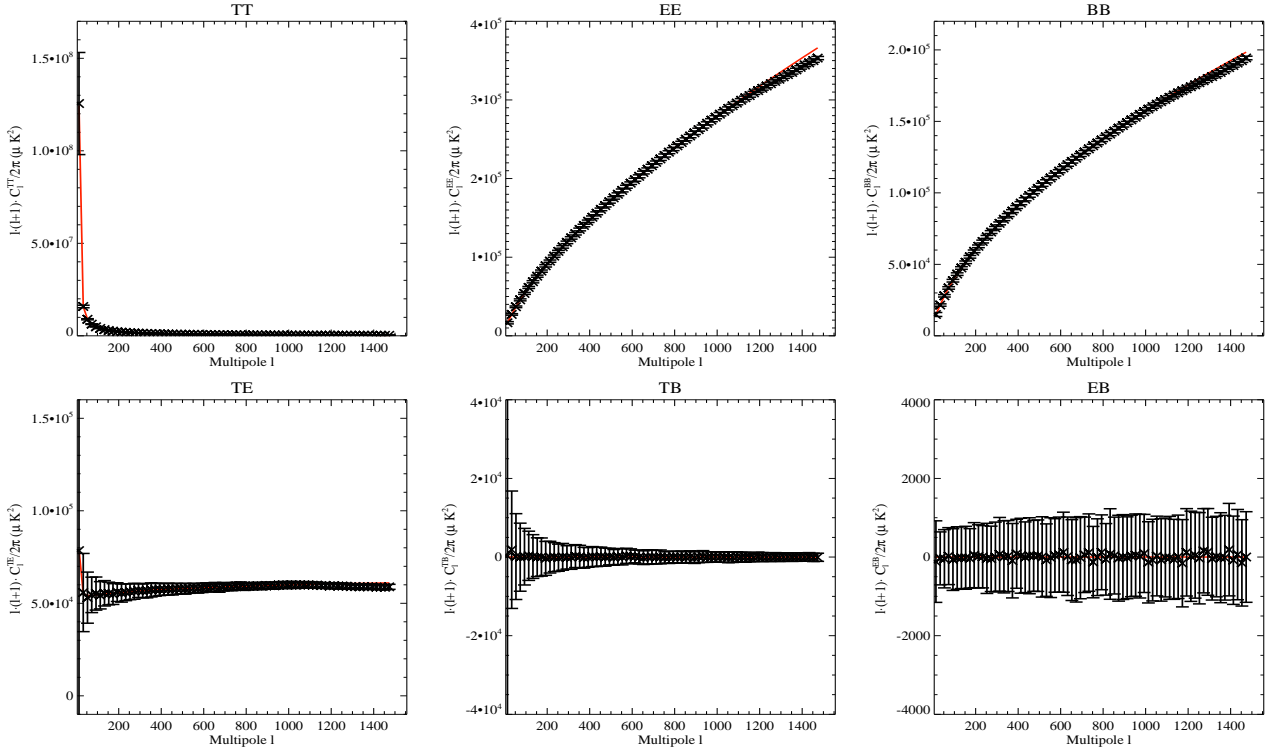


Figure 9. Same as figure 2 but for the [planck a] simulations for a CMB semi-blind analysis.

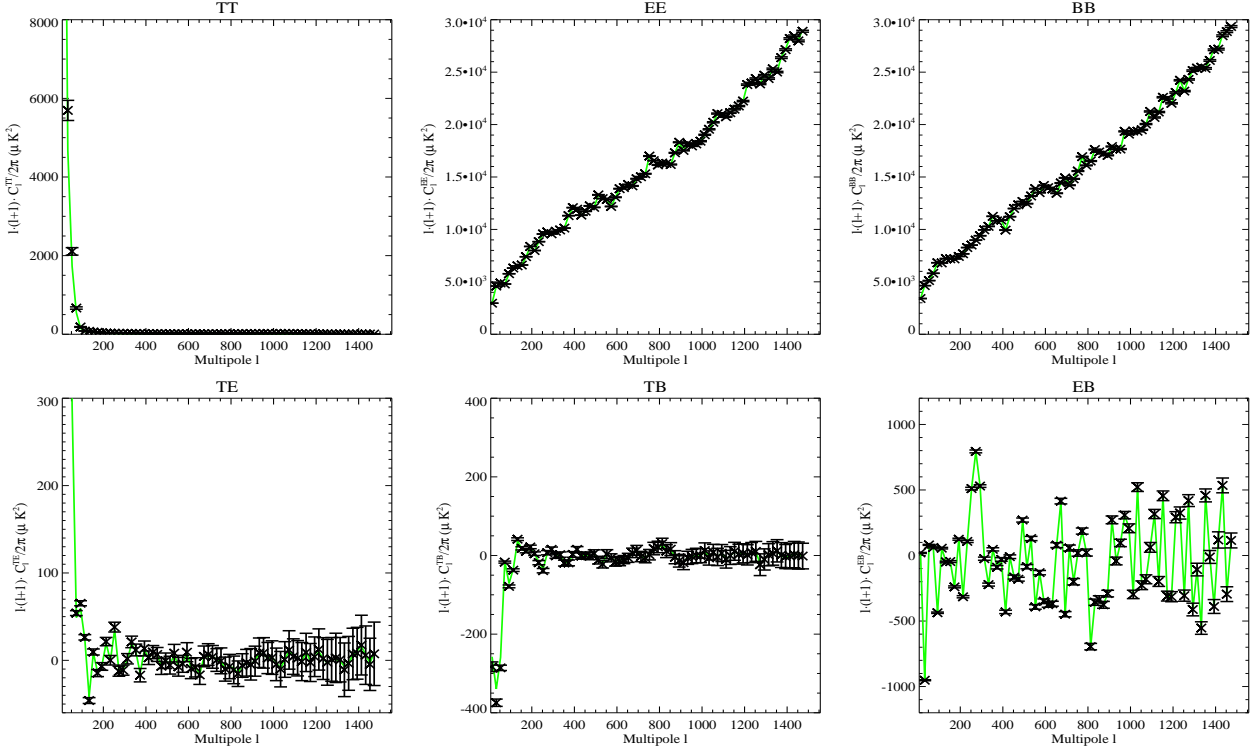


Figure 10. Same as figure 3 but for the [planck a] simulations for a CMB semi-blind analysis.

tion of the spatial power spectra was limited to $\ell = 383$. In some cases we have observed small biases in the polarization auto power spectra at large ℓ values which may be due to pixelization problems (we exclude in here the bias observed in the CMB *BB* modes which is due to residual noise). To check this hypothesis we have also performed the *blind*, *CMB semi-blind* and *A-fixed* analysis on the [planck a] simulations for which we can reconstruct the angular power spectra up to $\ell = 1535$. As the resolution of the Planck best channels is ~ 5 arcmin a more realistic analysis will require simulations at $n_{side} = 2048$ which are far too much time demanding for our computational capabilities.

The results obtained for the [planck a] simulations are very similar to those for the [planck c] ones. For illustration figures 8, 9 and 10 show the reconstructed temperature and polarization power spectra for CMB, dust and synchrotron in the case of a *CMB semi-blind* analysis. The synchrotron and dust power spectra are accurately reconstructed in temperature and polarization. We observe a slight bias in the dust *EE* and *BB* modes as for the [planck c] simulations but at much larger ℓ values. This indicates that this bias is related to pixelization effects. The same effect is observed for the CMB power spectra. The bias in the *EE* modes is present at much larger ℓ than for the [planck c] simulations. The reconstruction of the CMB *BB* modes is accurate at low ℓ ($\ell < 60$) and present a residual noise bias at large ℓ values as discussed in the previous section.

6.2 Color noise model

As seen before, the bias observed in the CMB *BB* power spectrum is most probably due to residual noise. Therefore, it is interesting to check both the accuracy of the noise reconstruction and the limitations of the white noise model imposed. With respect to the latter we have repeated all the analysis presented above assuming a color noise model such that the noise power spectra are estimated for each bin b in ℓ . For the *blind* analysis the results are slightly worse in the sense that the mixing up between CMB and synchrotron is more significant. This is not surprising since the noise in the data is white and we are artificially reducing the number of degrees of freedom in the fit. Actually, the mismatch between the data and the physical component power spectra can be compensated by changing the noise power spectra. In the case of the *CMB semi-blind* and *A-fixed* analysis the results for the white and color noise model present no significant differences.

Figure 11 shows, in black, the reconstructed noise angular power spectra, $C_{\ell}^{N,TT}$, $C_{\ell}^{N,EE}$, $C_{\ell}^{N,BB}$, in $\mu\text{K}_{\text{CMB}}^2$, at 100 GHz for the [planck a] simulations in the case of a *CMB semi-blind* analysis. We overplot, in black, the power spectra of the noise at 100 GHz obtained from 100 realizations of noise-only maps. The noise spectra are reconstructed down to the accuracy of the estimation of the input model both for *TT* and *EE*, well below 10^{-3} %. For the *BB* noise spectrum there is a small bias which is of the order of 5×10^{-3} % at $\ell = 200$ and around 2×10^{-2} % at $\ell = 1500$.

Therefore, to improve the reconstruction of the CMB *BB* modes we need a better estimation of the *BB* noise power spectrum. For this purpose we need to improve the likelihood maximization algorithm. For temperature-only separation, (Delabrouille et al. 2003) complemented the EM algorithm with a direct maximization of the likelihood function via a Newton-Raphson algorithm. For polarization similar algorithms can be used but due to the degree of complexity of the problem (6 correlated modes per physical component instead of 1 in the temperature only

case) and for the sake of clarity these will be discussed in a forthcoming paper.

6.3 Impact of foregrounds in the reconstruction of the CMB angular power spectra

In the previous sections we have shown that the PoLEMICA method is able to separate foregrounds and CMB signal both in temperature and polarization. However the presence of foregrounds limits the accuracy to which the CMB power spectra can be reconstructed. In other words, although the presence of foregrounds does not bias the recovered spectra their error bars increase significantly. This can be observed on figure 12 where we represent the error bars of the reconstructed CMB power spectra for the three types of analysis presented above. We trace in green the error bars for a *A-fixed* analysis of the [planck b] simulations which only include CMB signal. As no foreground signal is present we consider these error bars as the best we can obtain for the noisy data set. In blue and red we represent respectively the error bars for the *CMB semi-blind* and *blind* analysis of the [planck c] simulations including CMB and foregrounds.

From the figure we clearly observe that the presence of foregrounds increases by a factor of at least two the error bars in the reconstructed CMB power spectra both in temperature and polarization. For the *TT* and *TE* modes the *CMB semi-blind* and *blind* analysis give very similar error bars. For the *EE* modes the *blind* analysis leads to a factor of two larger error bars with respect to the *CMB semi-blind* one. In the case of the *blind* analysis there is no reconstruction of the *BB* modes and therefore the error bars are much larger, about a factor of 15 with respect to the CMB only case. Because of the uncertainties in the reconstruction of the *B* signal, the error bars for the *blind* reconstruction of *TB* and *EB* are 2.5 larger than for the *CMB semi-blind* case.

Notice that the impact of foregrounds on the reconstruction of the CMB temperature and polarization power spectra certainly depends significantly on the exact nature of the foregrounds as well as on the instrumental characteristics. We consider here a simple model for the sky emission with only three polarized components CMB, dust (Gaussian model) and synchrotron, no systematic effects, white noise, perfect absolute calibration and infinite resolution.

7 SUMMARY AND CONCLUSIONS

We present in this paper the PoLEMICA algorithm which is an extension to polarization of the SMICA temperature MD-MC blind component separation method developed by (Delabrouille et al. 2003). Both algorithms works in harmonic space and are based on the spectral matching of the data to a noisy linear mixture of physical components using the EM algorithm to maximize the likelihood function. By contrast to the temperature data which are described by a single scalar quantity T , the combined temperature and polarization data are described in harmonic space by three correlated scalar quantities T , E and B corresponding to the I , Q and U Stokes parameters in real space. We have developed a new formalism to jointly deal with the 6 resulting auto and cross angular power spectra, *TT*, *EE*, *BB*, *TE*, *TB* and *EB*.

Using this formalism we have constructed the likelihood function and proved that the EM algorithm can be also applied to polarization data. Under the assumption of Gaussian distributed components and noise, the free parameters in the fit are the mixing

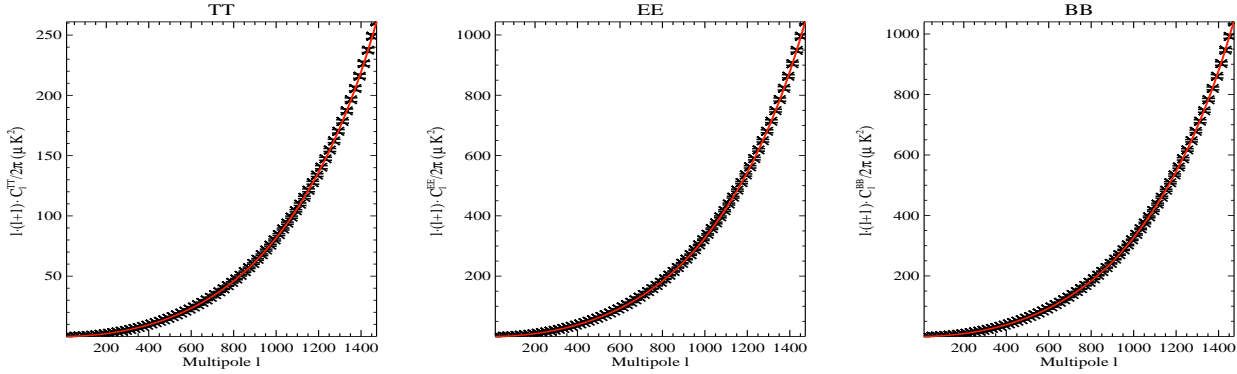


Figure 11. Reconstructed noise angular auto power spectra (black), in $\mu\text{K}_{\text{CMB}}^2$, at 100 GHz for T , E and B for the [planck a] simulations in the case of a *CMB semi-blind* separation. We overplot in red the noise auto power spectra at 100 GHz as obtained from 100 realizations of noise-only maps.

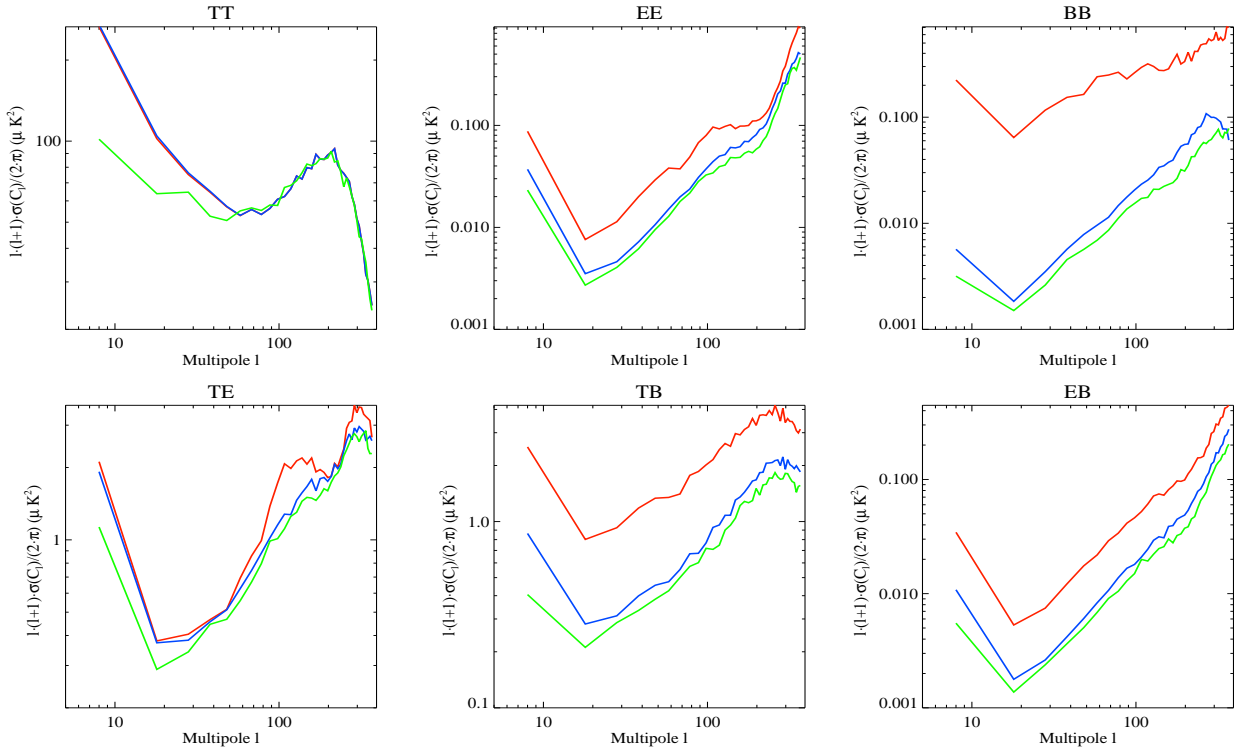


Figure 12. Error bars in the reconstruction of the CMB temperature and polarization power spectra at 100 GHz in $\mu\text{K}_{\text{CMB}}^2$. The green curve corresponds to the *A-fixed* analysis of the [planck b] simulations which includes only CMB. The blue and red curves correspond to the *CMB semi-blind* and *blind* analysis of the [planck c] simulations which include CMB, dust and synchrotron.

matrix describing the electromagnetic spectrum of the physical components for T , E and B , the temperature and polarization angular power spectra of the physical components and the temperature and polarization noise power spectra for each of the detectors.

We have successfully tested the PoLEMICA method on simulations of the Planck satellite experiment considering a 14-months nominal mission and no systematic effects. We suppose a simple linear model for the sky emission including CMB, synchrotron with constant spectral index and dust emissions. We construct full sky maps for all the polarized channels from 30 to 353 GHz including at least one of the above physical components and considering white noise and infinite resolution.

The method permits blind separation on these simulations allowing us to reconstruct the noise and physical component's temperature and polarization power spectra as well as the mixing matrix when we consider equal electromagnetic spectrum in T , E and B . When we relax this hypothesis the reconstruction of the electromagnetic spectrum for the CMB B modes is significantly degraded as could be expected because of the low signal to noise ratio. These results indicate that the PoLEMICA method allows us to both constrain the electromagnetic spectrum of the physical components and also to intercalibrate the data based on the reconstructed CMB electromagnetic spectrum.

To evaluate the impact of foregrounds in the determination

of the CMB temperature and polarization power spectra we have compared the results of the analysis on CMB only and CMB plus foregrounds simulations. In the presence of foregrounds, the error bars on the reconstruction of the CMB power spectra are increased by at least a factor of two both in temperature and in polarization even if we consider a *CMB semi-blind* analysis assuming the CMB electromagnetic spectrum known. Therefore, although the foreground contribution in the data can be removed, it significantly reduces the precision to which the CMB polarization signal can be extracted from the data. For a *blind* analysis the error bars are larger indicating that the use of prior information is badly needed for the analysis of future CMB data sets.

Finally, real experiments present finite resolution, partial effective sky coverage, systematic effects and, often, correlated noise. All these issues must be dealt with by the component separation algorithms and will with no doubt significantly limit the precision to which the CMB signal may be reconstructed. PoLEMICA, as it was already the case for SMICA, can account for beam and filtering smoothing. Furthermore, systematic effects and correlated noise can be modeled as extra components in the data for which the spectral dependence can be estimated in a *blind* analysis. In addition, foreground emissions have in general spatially varying electromagnetic spectra far beyond the simple linear model presented here. Work is in progress to adapt PoLEMICA to the case of foregrounds with spatially varying electromagnetic spectrum.

ACKNOWLEDGMENTS

We would like to thank D. Santos and F.X. Désert for very useful comments and a careful reading of the paper. Special thanks to M. Tristram for his comments and power spectrum related procedures and to D. Blais for his useful advises on matrix derivation. We acknowledge J.F. Cardoso, J. Delabrouille and G. Patanchon for comments on the technical details of the algorithm. The HEALPix package (Górski et al. 1999) was used extensively in this paper.

REFERENCES

- Baccigalupi C., 2004, MNRAS, 354, 5570
 Barkats D., Bischoff C., Farese P. et al., 2005, ApJ, 619, 127
 Bennett C. L. et al., 2003a, ApJS, 148, 1
 Bennett C. L. et al., 2003b, ApJS, 148, 97
 Benoît A. et al., 2003, A&A, 399, 19
 Benoît A. et al., 2004, A&A, 424, 571
 Bouchet F. R., Benoît A., Camus Ph., Désert F.X., Piat M. & Ponthieu N., 2005, SF2A 2005 proceedings, 675
 Bouchet F. R., Prunet S. & Sethi S. K., 1999, MNRAS, 302, 663
 Challinor A. & Chon G., 2002, Phys. Rev. D, 66, 127301
 deBernardis P. et al., 2000, Nat, 404, 955
 Delabrouille J., Cardoso J.-F. & Patanchon G., 2003, MNRAS, 346, 1089
 Dempster A., Laird N. & Rubin D., 1977, J. of the Roy. Stat. Soc. B, 39, 1
 Duncan A. R., Haynes R. F., Jones K. L. & Stewart R. T., 1997, MNRAS, 291, 279
 Eriksen H. K. et al., 2005, ApJ, submitted, astro-ph/0508268
 Finkbeiner D. P., Davies M. & Schlegel D.J., 1999, ApJ, 524, 857
 Giardino G., Banday A. J., Górska K. M., Bennet K., Jonas J. L. & Tauber J., 2002, A&A, 387, 82
 Górski K. M., Hivon E. & Wandelt B. D., 1999, astro-ph/9812350
 Halverson N. W. et al., 2002, ApJ, 568, 38
 Hanany S. et al., 2000, ApJ, 545, 5
 Haslam C. G. T., Stoffel H., Salter C. J. & Wilson W. E., 1982, A&AS, 47, 1
 Hildebrand R. H., 1996, In polarimetry of the interstellar Medium, Roberge W.G., Whittet D.C.B. (eds), ASP Conference Series, 97, 254
 Hinshaw G. et al., 2003, ApJS, 148, 135
 Hobson M. P., Jones A. W., Lasenby A. N. & Bouchet F., 1998, MNRAS, 300, 1
 Hu W., 2000, Phys. Rev. D, 62, 043007
 Jones W. C et al., 2005, ApJ, submitted, astro-ph/0507494
 Kogut A., Spergel D. N., Barnes C., 2003, ApJS, 148, 161
 Kovac J., Leitch E. M., Pryke C. et al., 2002, Nat, 420, 772
 Knox L. & Turner S., 1994, Phys. Rev. Lett., 73, 3347
 Lagache G., 2003, A&A, 405, 813
 Lee A. T. et al., 2001, ApJ, 561, 1
 Leitch E. M., Kovac J., Halverson N. et al., 2005, ApJ, 624, 10
 Lewis A., Challinor A. & Lasenby A., 2000, ApJ, 538, 473
 Maino D. et al., 2002, MNRAS, 334, 53
 Miller A. D. et al., 1999, ApJ, 524, 1
 Montroy T. E. et al., 2005, ApJ, submitted, astro-ph/0507514
 Netterfield C. B. et al., 1997, ApJ, 474, 47
 Netterfield C. B. et al., 2002, ApJ, 571, 604
 Okamoto T. & Hu W., 2003, Phys. Rev. D, 67, 083002
 Piacentini F. et al., 2005, ApJ, submitted, astro-ph/0507507
 Planck Consortium, 2005, ESA Publications Division
 Ponthieu N. et al., 2005, A&A, 444, 327
 Prunet S., Sethi S. K., Bouchet F. R. & Miville-Deschéne M. -A., 1998, A&A, 339, 187
 Readhead A., Myers S., Pearson T. et al., 2004, Science, 306, 836
 Rubino-Martin J. A. et al., 2003, MNRAS, 341, 1084
 Seljak U., Hirata C. H., 2004, Phys. Rev. D, 69, 4
 Schlegel D. J., Finkbeiner D. P. & Davies M., 1998, ApJ, 500, 525
 Sievers J. L. et al., 2003, ApJ, 591, 599
 Smoot G. F. et al. 1992, ApJ, 396, 1
 Snoussi H., Patanchon G., Macías-Pérez J.-F., Mohammad-Djafari A. & Delabrouille J., 2001, Am. Inst. of Phys. Baltimore, Bayesian Inference and Maximum Entropy Methods in Science Engineering 125-140, MAXENT 2001
 Spergel D. N. et al., 2003, ApJS, 148, 175
 Stolyarov V., Hobson M. P., Ashdown M. A. J. & Lasenby A. N., 2002, MNRAS, 336, 97
 Stolyarov V., Hobson M. P., Lasenby A. N. & Barreiro R. B., 2005, MNRAS, 357, 145
 Tegmark M. & Efstathiou G., 1996, MNRAS, 281, 1297
 Tristram M. et al., 2005, A&A, 436, 785
 Tucci M., Martínez-González E., Gonzalez-Nuevo J. & De Zotti G., 2004, MNRAS, 349, 1267
 Tucci M., Martínez-González E., Vielva P. & Delabrouille J., 2005, MNRAS, 360, 926
 Turner M. S. & White M., 1996, Phys. Rev. D, 53, 6822
 Wolleben M., Landecker T. L., Reich W. & Wielebinski R., 2005, A&A, submitted, astro-ph/0510456
 Zaldarriaga M. & Seljak U., 1997, Phys. Rev. D, 55, 1830
 Zaldarriaga M., Spergel D. N. & Seljak U., 1997, ApJ, 488, 1

APPENDIX A: MD-MC POLARIZATION SKY MODEL

We discuss here the formalism developed to describe the temperature and polarization observations as a noisy mixture of independent components.

In the following we assume full sky observations at two frequencies ν_1 and ν_2 and a simple linear model for the sky emission with two components c_1 and c_2 .

In this case, equation (2) reads

$$\begin{pmatrix} y_{\ell m}^{v_1 T} \\ y_{\ell m}^{v_1 E} \\ y_{\ell m}^{v_1 B} \\ y_{\ell m}^{v_2 T} \\ y_{\ell m}^{v_2 E} \\ y_{\ell m}^{v_2 B} \\ y_{\ell m}^{v_2 C} \end{pmatrix} = \begin{pmatrix} f_{v_1 c_1}^T & 0 & 0 & f_{v_1 c_2}^T & 0 & 0 \\ 0 & f_{v_1 c_1}^E & 0 & f_{v_1 c_2}^E & 0 & 0 \\ 0 & 0 & f_{v_1 c_1}^B & 0 & 0 & f_{v_1 c_2}^B \\ f_{v_2 c_1}^T & 0 & 0 & f_{v_2 c_2}^T & 0 & 0 \\ 0 & f_{v_2 c_1}^E & 0 & 0 & f_{v_2 c_2}^E & 0 \\ 0 & 0 & f_{v_2 c_1}^B & 0 & 0 & f_{v_2 c_2}^B \end{pmatrix} \cdot \begin{pmatrix} s_{\ell m}^{v_1 T} \\ s_{\ell m}^{v_1 E} \\ s_{\ell m}^{v_1 B} \\ s_{\ell m}^{v_2 T} \\ s_{\ell m}^{v_2 E} \\ s_{\ell m}^{v_2 B} \\ s_{\ell m}^{v_2 C} \end{pmatrix} + \begin{pmatrix} n_{\ell m}^{v_1 T} \\ n_{\ell m}^{v_1 E} \\ n_{\ell m}^{v_1 B} \\ n_{\ell m}^{v_2 T} \\ n_{\ell m}^{v_2 E} \\ n_{\ell m}^{v_2 B} \\ n_{\ell m}^{v_2 C} \end{pmatrix}$$

where $y_{\ell m}^{v_i X}$ and $s_{\ell m}^{c_j X}$ for $X = \{T, E, B\}$ are the coefficients of the spherical harmonic decomposition of the input sky observations and of the components of the sky model respectively. The coefficients $f_{v_i c_j}^X$ correspond to the electromagnetic spectrum of the component c_j at the frequency of observation v_i . Note that the mixing matrix, A , has dimensions $3 \cdot n_v \times 3 \cdot n_c$.

We define the noise, $R_n(b)$, signal, $R_s(b)$, and data, $R_y(b)$, density matrices used in equation (5) for each bin, b , as follows

$$R_z(b) \equiv \frac{1}{n_b} \sum_{\vec{\ell} \in \mathcal{D}_b} \langle z(\vec{\ell}) z(\vec{\ell})^\dagger \rangle, \quad z = \{n, s, y\}$$

Assuming the noise uncorrelated between detectors the noise density matrix is diagonal

$$R_n(b) = \begin{pmatrix} & & \nu_1 & & \nu_2 \\ & N_\ell^{TT}(b) & & & \\ \nu_1 & & N_\ell^{EE}(b) & & 0 \\ & & & N_\ell^{BB}(b) & \\ & & 0 & & N_\ell^{TT}(b) \\ & & & & N_\ell^{EE}(b) \\ \nu_2 & & & & N_\ell^{BB}(b) \end{pmatrix}$$

In the same way assuming independent physical components the signal density matrix is block diagonal and reads

$$R_s(b) = \begin{pmatrix} c_1 & \begin{bmatrix} S_{\ell}^{TT}(b) & S_{\ell}^{TE}(b) & S_{\ell}^{TB}(b) \\ S_{\ell}^{TE}(b) & S_{\ell}^{EE}(b) & S_{\ell}^{EB}(b) \\ S_{\ell}^{TB}(b) & S_{\ell}^{EB}(b) & S_{\ell}^{BB}(b) \end{bmatrix} & c_2 \\ c_2 & 0 & \begin{bmatrix} S_{\ell}^{TT}(b) & S_{\ell}^{TE}(b) & S_{\ell}^{TB}(b) \\ S_{\ell}^{TE}(b) & S_{\ell}^{EE}(b) & S_{\ell}^{EB}(b) \\ S_{\ell}^{TB}(b) & S_{\ell}^{EB}(b) & S_{\ell}^{BB}(b) \end{bmatrix} \end{pmatrix}$$

Finally the data density matrix can be written by blocks as follows

$$R_y(b) = \begin{pmatrix} & \begin{bmatrix} & \nu_1 & \\ Y_\ell^{TT}(b) & Y_\ell^{TE}(b) & Y_\ell^{TB}(b) \\ Y_\ell^{TE}(b) & Y_\ell^{EE}(b) & Y_\ell^{EB}(b) \\ Y_\ell^{TB}(b) & Y_\ell^{EB}(b) & Y_\ell^{BB}(b) \\ Y_\ell^{TT}(b) & Y_\ell^{TE}(b) & Y_\ell^{TB}(b) \\ Y_\ell^{TE}(b) & Y_\ell^{EE}(b) & Y_\ell^{EB}(b) \\ Y_\ell^{TB}(b) & Y_\ell^{EB}(b) & Y_\ell^{BB}(b) \end{bmatrix} & \begin{bmatrix} & \nu_2 & \\ Y_\ell^{TT}(b) & Y_\ell^{TE}(b) & Y_\ell^{TB}(b) \\ Y_\ell^{TE}(b) & Y_\ell^{EE}(b) & Y_\ell^{EB}(b) \\ Y_\ell^{TB}(b) & Y_\ell^{EB}(b) & Y_\ell^{BB}(b) \\ Y_\ell^{TT}(b) & Y_\ell^{TE}(b) & Y_\ell^{TB}(b) \\ Y_\ell^{TE}(b) & Y_\ell^{EE}(b) & Y_\ell^{EB}(b) \\ Y_\ell^{TB}(b) & Y_\ell^{EB}(b) & Y_\ell^{BB}(b) \end{bmatrix} \\ \nu_1 & & \\ & & \\ \nu_2 & & \end{pmatrix}$$